

## Investigation of the structure-transport correlation in metal phthalocyanine thin films

Sabyasachi Karmakar<sup>1,2</sup>, Mrinmay K. Mukhopadhyay<sup>1,2,\*</sup> and Milan K. Sanyal<sup>1</sup><sup>1</sup>*SPMS Division, Saha Institute of Nuclear Physics, 1/AF Bidhannagar, Kolkata 700064, India*<sup>2</sup>*Homi Bhabha National Institute, BARC Training School Complex, Anushaktinagar, Mumbai 400094, India* (Received 17 October 2023; revised 5 January 2024; accepted 18 January 2024; published 8 February 2024)

The correlation of thin films structure and orientation of small organic molecules with the physical properties like charge carrier transport is not only important for basic understanding but also crucial for various application as functional devices. Small organic semiconductor molecules assemble in different configuration in thin films resulting in exhibiting a wide variety of optoelectronic properties. Here, we have investigated the structure of thin films of three metal phthalocyanines (MPcs) having a metal ion as Cu, Co, and Ni using a combination of x-ray scattering techniques and microscopic images. The x-ray results reveal that the molecules assemble in sticklike nanograins of well-ordered structure on Si surface. These nanograins packed differently for three different metal ions and CuPc growth are more of a columnar type whereas NiPc form much smoother films. The *I-V* measurements reveal higher conductivity for the thinner films, both under optical illumination and dark condition, in contrary to the normal convention. This observation was explained in terms of the transport of carriers through the region of trapped charge states in the ordered phase of the nanograins and the porous region between the grains resulting in different threshold voltages for differently ordered films.

DOI: [10.1103/PhysRevMaterials.8.024601](https://doi.org/10.1103/PhysRevMaterials.8.024601)

## I. INTRODUCTION

Organic semiconductors (OSCs) have received enormous attention due to their physical, optical, and electronic properties suitable for various optoelectronic device applications. Over the last decades organic small molecular materials have emerged as the platform to explore the spin-dependent transport in the nanoscale with a wide range of potential applications starting from data storage devices [1,2], spintronic devices with magnetic sensitivity [3], and many others. The inexpensive nature of most of the OSC materials, easy way of large-scale production, and mechanical flexibility make them eligible for low-cost device fabrication. There are several such materials like  $\pi$ -conjugated small chain polymers [4,5], fullerenes [6,7], etc., and metal phthalocyanines (MPcs) are one of the very important members of this OSC family. MPcs have a highly conjugated cyclic structure with a central chelated metal ion which consists of four isoindole groups corresponding to 18  $\pi$  electrons [8]. MPcs are successfully used in various electronic devices including organic light emitting diodes (OLEDs), organic solar cells, and organic field effect transistors (OFETs) [9,10]. MPcs are also under intensive investigation to fabricate spin-dependent devices such as organic spin valves (OSVs), OLED-based magnetic sensors, and spin-OLEDs [10,11].

MPcs can exist in different polymorphic forms like  $\alpha$ ,  $\beta$ ,  $\gamma$ , etc. [8]. Among all these phases, the metastable  $\alpha$  and stable  $\beta$  phases are the most common and significant for device applications. The transformation from  $\alpha$  to  $\beta$  mainly depends on substrate temperature and can be distinguished by their

molecular packing and tilt angle. It is known that the molecular orientation and ordering of this kind of small molecular thin films play a very crucial role in functionality and efficiency of a device [12–20]. Such films can be easily deposited using simple thermal evaporation technique [21–24]. Thin-film morphology is mainly affected by parameters like deposition rate, substrate temperature, and surface energy of a substrate [8,25] which results in forming microstructures of different sizes ranging from single crystal to amorphous. At elevated substrate temperatures, molecules have enough kinetic energy to migrate to lower energy sites creating nucleation points, resulting in polycrystalline structures with large crystallites, and fewer grain boundaries [8,26–28]. Nucleation density is also affected by deposition rate and subsequently dictates crystallite size leading to different morphology [8,29–32]. It is predicted that the layer-by-layer growth of such thin films is possible when the surface free energy of the substrate is more than that of the film and interface. On the other hand, the island-type growth will be the dominant feature when the surface free energy of the substrate is smaller than that of the film and interface [33]. Depending on the substrate surface, different MPc molecules can orient differently in columnlike or horizontally aligned manner [13–15]. Weak interaction between the molecule and the substrate results in vertical stacking of the molecules, whereas some MPc molecules can cover the whole substrate surface reducing the total surface energy [34–37]. In thicker films, molecules start to transform from the surface structure to bulk structure by strain relaxation mechanism and the morphology of the initial growth process dictates further growth in thin film systems [38,39]. It is known that relative sizes between the cavity of the phthalocyanine ring and central metal ion determine the structure of MPcs. Different central metal atoms can result

\*Corresponding author: [mrinmay.mukhopadhyay@saha.ac.in](mailto:mrinmay.mukhopadhyay@saha.ac.in)

in either ring contraction, ring expansion, or ring doming in MPcs and some metal ions like Cu and Co take cavity diameter close to that of the equilibrium metal-free phthalocyanine [8,40]. Szybowicz *et al.* have demonstrated a clear change in the metal-dependent band around  $1500\text{ cm}^{-1}$  for different MPcs using polarized Raman spectroscopy [8,41,42]. This change also affects the molecular packing, organization, and also change in angle between MPc molecules and the substrate. Despite all these previous results, the morphology and the orientation of different MPc molecules at the initial growth state are not clear yet. Mostly, the morphological studies on the initial growth mode of MPc thin films were performed by atomic force microscopy (AFM) or transmission electron microscopy (TEM) measurement [34–37]. But only AFM or TEM measurements are not useful to get information about molecular orientation inside the film and also the conventional x-ray diffraction (XRD) is not good enough to probe the structure due to the small amount of materials in thin-film configuration and the low-scattering cross section of organic components.

MPc-based devices exhibit different performance depending on the nature of the central metal atom [43]. The transition metal (Fe, Co, Ni, Cu, Zn) phthalocyanines have the same molecular structure and symmetry [43,44]. In this article, we report detailed growth and structural evolution of CuPc, CoPc, and NiPc thin films on silicon substrate by varying thickness and have shown the effect of thickness and morphology variation in charge-carrier transport by measuring the  $I$ - $V$  characteristics from these films. The out-of-plane and in-plane structure of the thin films were obtained using x-ray reflectivity (XRR) and grazing incidence small-angle x-ray scattering (GISAXS) measurement respectively. The x-ray scattering results show MPc molecules grow as sticklike nanograins on the Si surface and the assembly of these grains varies for different MPcs where CuPc molecules form more like a columnar structure and NiPc films form smoother films. The in-plane morphology measured using AFM corroborates the extracted in-plane structure from the GISAXS measurement. A model has been predicted to establish a correlation in charge-carrier transport of these films having different thicknesses with the structure and morphology of the molecular assembly. Such a correlation between the structure at the initial growth process in thin films with the transport properties will help us to engineer various optoelectronic devices for wide range of applications.

## II. EXPERIMENTAL DETAILS

Metal-Pc (MPc) chemicals, namely CuPc (99.9% pure), CoPc (97%), NiPc(97%) have been purchased from Sigma Aldrich and used with no further purification process. Silicon wafers (*p*-type, (100)) have been purchased from Sigma Aldrich. Wafers were cleaned in an ultrasonic bath with acetone, 2-propanol, and DI water successively. Before loading into the chamber, all substrates were dried by using dry  $\text{N}_2$  gas. Thermal evaporation was performed at  $5.0 \times 10^{-6}$  Torr pressure and at a rate of  $0.15\text{ \AA/s}$ . A substrate temperature of 373 K was maintained during evaporation. We have deposited four different types of thickness for each Pc's and they are denoted as A, B, C, and D in ascending

order of thickness. X-ray reflectivity and diffraction were performed using a Rigaku Smart Lab instrument at wavelength  $1.54\text{ \AA}$ . GISAXS was performed in the Indian Beamline at Photon Factory (BL-18B), KEK, Japan with incident energy of 12 keV and the scattered beam was imaged with a Pilatus 1M detector. The distance from the sample to the detector was 3.6 m for the GISAXS measurement. AFM was performed in tapping mode using a CSI nano-observer instrument. We have used WSxM software for image processing and to extract power spectral density (PSD) profiles from the images. SEM images were taken using a Supra 40 FESEM instrument with accelerating voltage at 5 kV. For electrical measurement, we have fabricated two-terminal devices with a channel length of  $\sim 200\text{ }\mu\text{m}$ . First, we patterned  $\text{SiO}_2$  substrates ( $10 \times 10\text{ mm}$ ) using photolithography and then a Ti/Au electrode was deposited using e-beam evaporation. Over these patterned substrates, an organic layer was deposited to fabricate the device. The  $I$ - $V$  characteristics were performed using a Keithley 2602 source meter and an UV lamp was used for the photoconductivity measurement.

## III. RESULTS AND DISCUSSION

XRR, a well-known nondestructive technique, has been used to investigate the out-of-plane structure of the deposited thin films which gives us the information of electron density profile (EDP) as a function of the film thickness [45]. The fitted EDP provides us the model about the molecular arrangement in the vertical direction of the film and the roughness at the interfaces of the molecular stack along the film growth direction. XRR data and fitted curves for all the samples are shown in Figs. 1(a)–1(c). We have used Parratt formalism to fit the XRR data and extracted the EDPs from the fitted curves [45,46]. The thin films are modeled with multiple stacks of bilayer configuration and each of the bilayers consists of a high-density and low-density region. The roughness-convoluted periodic density variations throughout the thickness of the films are shown in Figs. 1(d)–1(f) and the orange curve in Fig. 1(d) shows the representative block of different density layers without the roughness convolution that we used for reflectivity calculation with Parratt formalism. This kind of periodic density variation gives us the XRR Bragg peaks at  $q_z$  value  $0.48\text{ \AA}^{-1}$  and the calculated thickness corresponding to that peak is about  $13\text{ \AA}$  which is a single molecular length in a tilted configuration and a gap between the stack of two molecules [20].  $\Delta q_z$  corresponding to two consecutive oscillations increases for the thinner films and for the lowest thickness CuPc film, the curve A in Fig. 1(a), the Bragg peak is broadened and only one oscillation can be measured after  $q_z = 0.6\text{ \AA}^{-1}$  before the reflectivity reaches the background [Fig. 1(a)]. The corresponding EDP profile (black curve) shows that the organic film thickness is around  $64\text{ \AA}$  and it consists of three well-defined molecular layers and two semifilled layers [Fig. 1(d)]. The thicknesses of the other three CuPc films (B–D) are 105, 180, and  $220\text{ \AA}$  respectively. It is clear from the XRR of CuPc films that the Bragg peak is getting sharper and Laue oscillations start to appear with the increase in film thickness. The fitted EDPs for the thicker films also show two partially filled molecular layers at the top but the layers underneath are mostly filled with well-organized

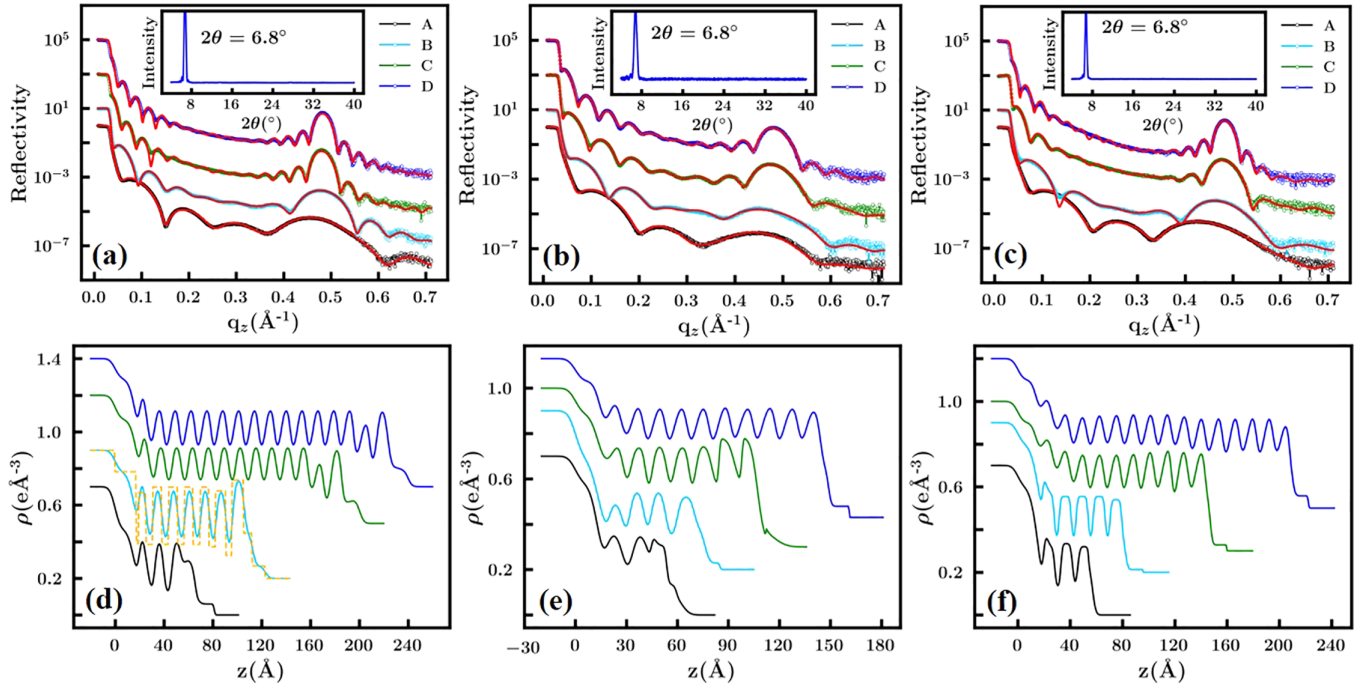


FIG. 1. (a)–(c) XRR profiles of CuPc, CoPc, and NiPc films. Experimental data (open circles), fitted curve (red line). (d)–(f) Extracted EDP profiles from the fitting of XRR of the corresponding films. Orange curve in (d) shows EDP profile without roughness convolution. Insets show the corresponding XRD profile of D films.

molecular arrangement and do not change much for the higher thickness of CuPc films. XRR profiles of CoPc films are shown in Fig. 1(b) and the corresponding EDP profiles are shown in Fig. 1(e). The thicknesses are coming out to be 51 Å, 71 Å, 102 Å, and 145 Å for the films A–D, respectively. In the case of NiPc, the XRR profiles and fitted EDPs give the thickness of these films as 50 Å, 80 Å, 144 Å, and 206 Å for films A–D, respectively, as shown in Fig. 1(c) and Fig. 1(f). It is important to note that only a small hump is visible after the Bragg peak for the thinner films (sample A and B) of CoPc and NiPc, whereas a clear reflectivity oscillation is present even for the thinner films (sample A and B) of CuPc. In the case of CoPc and NiPc films, reflectivity oscillations have started to appear on the right side of the Bragg peak for thicker films only, in contrary to the same for the CuPc films. So, in the earlier growth stage, the out-of-plane structure is a little distorted for thin films of all three materials and with increasing thickness this distortion reduces drastically. The presence of almost undamped oscillations (Laue oscillations) around the Bragg reflections for the thicker films is evidence of homogeneous coherent thickness, i.e., a well-defined out-of-plane structure [Figs. 1(a)–1(c)]. The calculated reflectivity profile matches well with the experimental data and also replicates exactly the Bragg peaks, and Kiessig and Laue oscillations in the XRR profiles. This is only possible when the out-of-plane structure grows along the substrate normal. So, an almost vertical columnar growth pattern is found to be the predominant growth mode in these thin films and CuPc is showing the most ordered vertical structure among these three materials. XRD profiles of thick (D) films are shown in the insets of Figs. 1(a)–1(c). All the profiles exhibit only one diffraction peak around  $2\theta = 6.8^\circ$ . This peak corresponds to the (200)

lattice plane of  $\alpha$  phase and it is consistent with the results found elsewhere [47–50].

In order to investigate the in-plane structure of the films of three different molecules, we have performed GISAXS experiment and the extracted line profiles from the GISAXS images of all the films are shown in Figs. 2(a)–2(c). The inset shows the 2D GISAXS image of the corresponding A-type films only. The GISAXS image shows a strong peak at  $q_y = 0$  and a pair of weak satellite peaks on each side of the main peak. These satellite peaks can be termed as the “in-plane correlation peak,” which signifies the presence of a 2D correlated in-plane structure caused by the lateral density modulations in the sample [51]. To estimate the shift in the in-plane correlation peaks for different samples, we have plotted the peak positions ( $q_y$ ) with corresponding film thickness ( $Z$ ) in Fig. (3). It is observed that the peak position shifts to higher  $q_y$  values with the increase in the film thickness for all three types of material indicating a larger separation between the correlated in-plane structure with the increase in film thickness.

In order to model the GISAXS data we have considered a simple one-dimensional “sticklike” shape function which is defined in Eq. (1) and the corresponding form factor in Eq. (2) [52]:

$$\mathcal{F}(x, L) = \begin{cases} \rho_0 & \text{if } |x| \leq L \\ 0 & \text{if } |x| > L, \end{cases} \quad (1)$$

$$F(q, L) = 2L\rho_0[\sin(qL)/qL], \quad (2)$$

where  $\rho_0$  is the electron density of the material. Now, if we consider that the size of these sticks follows a Gaussian

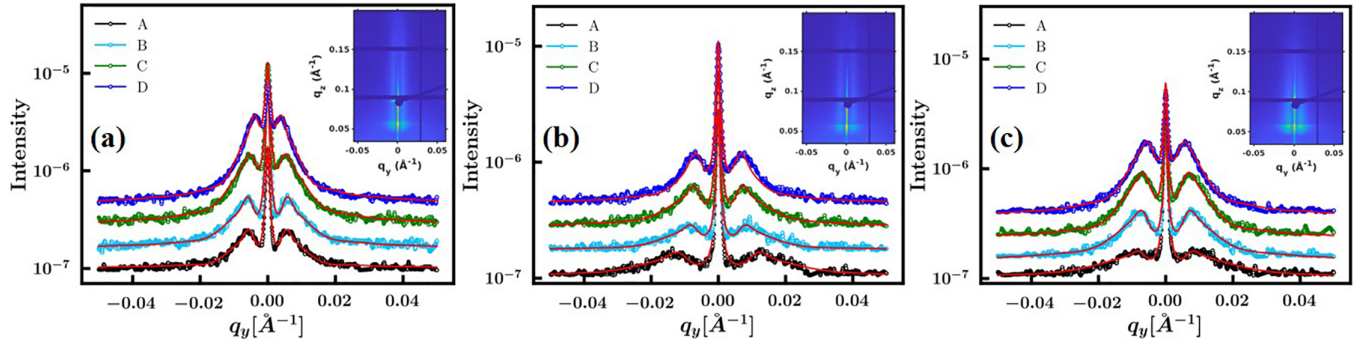


FIG. 2. (a)–(c) GISAXS line profiles of CuPc, CoPc, and NiPc samples. Experimental data (open circles), simulated curve (solid line), and insets show corresponding 2D GISAXS image of A films.

probability with a mean length  $L_0$  and standard deviation  $\sigma_L$  then it leads to as follows:

$$\langle |F(q, L)|^2 \rangle = \frac{2\rho_0^2}{q^2} [1 - \exp(-2\sigma_L^2 q^2) \cos(2qL_0)], \quad (3)$$

$$\langle |F(q, L)|^2 \rangle = \frac{4\rho_0^2}{q^2} \sin^2(qL_0) \exp(-q^2\sigma_L^2). \quad (4)$$

Assuming that the sticks are separated by a mean distance  $\xi$  with standard deviation  $\sigma_\xi$  and follows Gaussian probability, this leads to the expression in the  $q$  space as

$$P(q) = \exp\left(\frac{-q^2\sigma_\xi^2}{2}\right) \exp(iq\xi). \quad (5)$$

Writing  $P(q) = \phi(q) \exp(iq\xi)$ , we reach the expression of interference function of a one-dimensional Hosemann paracrystal equation [52,53]

$$S_\phi(q) = \frac{1 - \phi(q)^2}{1 + \phi(q)^2 - 2\phi(q) \cos(q\xi)}. \quad (6)$$

The total scattered intensity is then expressed as

$$I(q) = \Phi_0(q) + \langle |F(q, L)|^2 \rangle S_\phi(q) + G(q), \quad (7)$$

where  $\Phi_0(q) = \langle |F(q, L)|^2 \rangle - \langle |F(q, L)|^2 \rangle^2$  is the incoherent contribution due to the size distribution of the sticks and  $G(q)$  is a Gaussian peak added to simulate the central peak which arises due to substrate contribution at  $q_y = 0$ . Using Eq. (7)

we have calculated the scattered intensity as a function of  $q_y$  and the result is plotted in Fig. 2 (solid red lines). The parameters used to simulate the intensity are shown in Table I. We can see that the length  $L$  of the sticks as well as the interstick distance  $\xi$  both have quite a large deviation ( $\sigma_L$  and  $\sigma_\xi$ ) for all three types of samples. These deviations signify that the stick size and the distance between the sticks both have the Gaussian fluctuations around a peak value, and the peak width signifies the variation of random nature around that mean value. The average length of the sticks increases with thickness for all three types of samples. On the basis of these results, we propose a model of the initial growth mechanism of these films, and a schematic of that model with a detailed view of molecular assembly is shown in Fig. 3 (inset). Crystal structure analysis of a similar type of CuPc film is reported in Ref. [50] and shows that the lattice parameter  $a = 26.1 \text{ \AA}$ . This value of  $a$  is almost twice the value of our extracted bilayer thickness  $13 \text{ \AA}$ . This implies that for these films the  $a$  axis is aligned towards the normal to the substrate [50]. On Si surface, the molecules form well-ordered small crystalline nanodomains and these domains are separated by noncrystalline porous regions. If we consider the fitting parameters of  $L_0$  and  $\xi$  of the thickest film and the thinnest one for CuPc films, the increase in crystalline domain size and the noncrystalline domain size is almost in the same ratio. But in the case of CoPc and NiPc, the size of the crystalline domain increases almost double that of the noncrystalline domain size. These

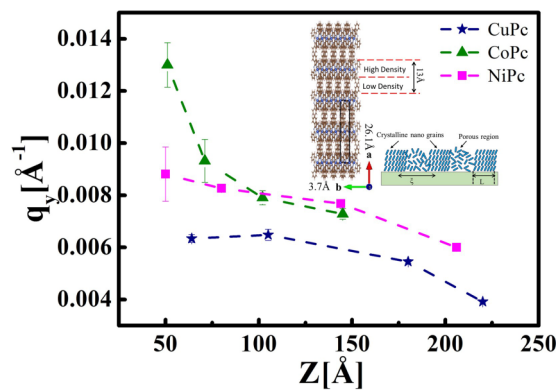


FIG. 3. Peak position in GISAXS vs thickness plot. Schematic of in-plane and out-of-plane molecular structures in thin film configuration is shown in the inset.

TABLE I. GISAXS line profile fitting parameters.

		$L_0(\text{\AA})$	$\sigma_L(\text{\AA})$	$\xi(\text{\AA})$	$\sigma_\xi(\text{\AA})$
CuPc	A	128	33	1018	304
	B	143	27	1061	323
	C	148	37	1111	386
	D	187	42	1597	386
CoPc	A	59	19	454	161
	B	92	21	678	246
	C	97	28	805	259
	D	141	40	832	273
NiPc	A	47	29	685	248
	B	98	31	765	284
	C	125	30	796	315
	D	142	37	935	429

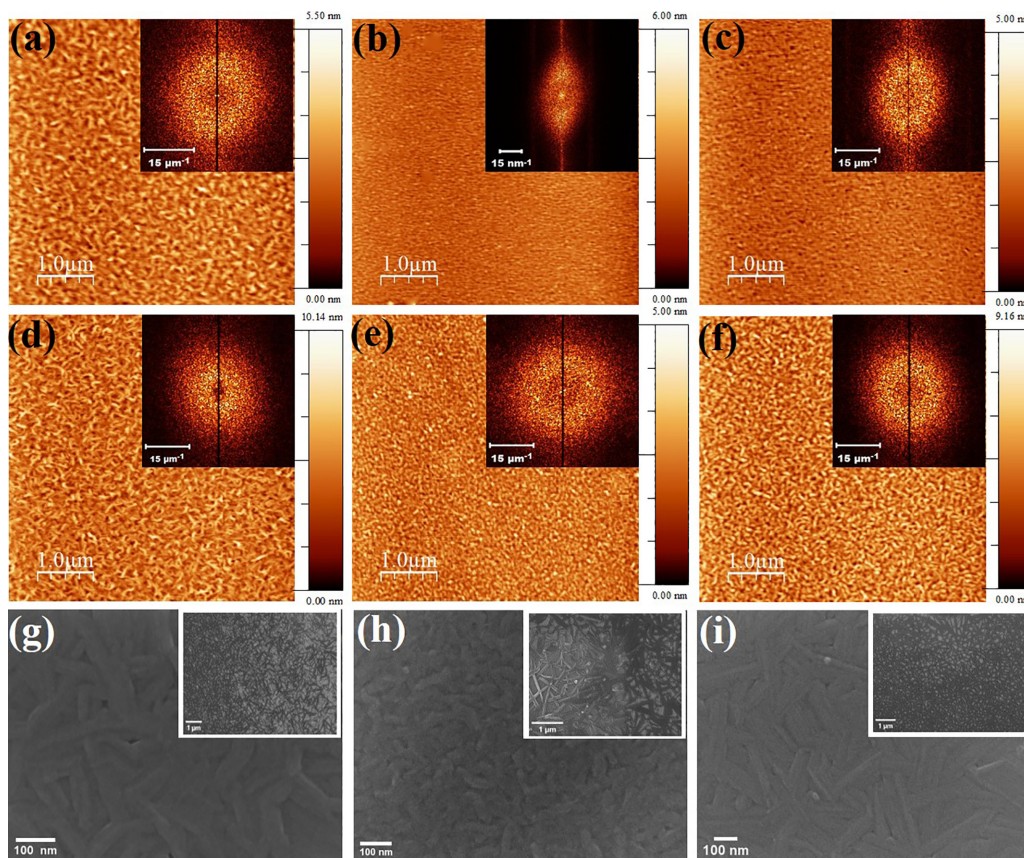


FIG. 4. (a)–(c) AFM images of B-type films of CuPc, CoPc, and NiPc. (d)–(f) AFM images of D-type films of CuPc, CoPc, and NiPc. Insets show corresponding FFT profiles. (g)–(i) SEM images of D-type films of CuPc, CoPc, and NiPc and corresponding insets show the images taken from the edges of the films.

in-plane structural differences between the films of CuPc and CoPc-NiPc have a clear signature in the  $I$ - $V$  measurements which will be explained later in the paper.

In order to investigate the surface morphology of the deposited films, AFM was performed and the images for one thin (B-type) and one thick (D-type) film for all three materials are shown in Figs. 4(a)–4(f). It can be clearly seen that in the initial growing period (B-type films), only the CuPc film exhibits a sticklike pattern but CoPc and NiPc films are more compact and uniform [Figs. 4(a)–4(c)]. But when the film thickness gradually increases, sticklike patterns gradually appear for all the materials and then become more and more clear as shown in Figs. 4(d)–4(f). The r.m.s. roughness we get from the thin samples (B-type films) are 7.1, 3.6, and 3.9 Å for CuPc, CoPc, and NiPc, respectively, and for the thick samples (D-type films) these values are 10.7, 5.6, and 12.5 Å. This roughness evolution and surface morphology of the film clearly indicate the columnar growth of molecules for the thicker films in particular. The FFT of the AFM images is shown in the insets of Fig. 4. The presence of circular symmetric spectra implies that the surface is isotropic (rotational invariance) [54] and the clear bright ringlike patterns indicate the presence of a characteristic length scale [55–57]. These patterns signify the possibility of the presence of a correlation between the sticklike features. To better estimate the in-plane correlated length scale from the AFM images, we have plotted the PSD profiles of corresponding AFM images, which are

shown in Fig. 5. It is known that the PSD profile is the angular average of the radial distribution of wavevector  $k$ . Here we have extracted the lateral correlation length by converting the characteristic bend, i.e., a major change in the slope in the

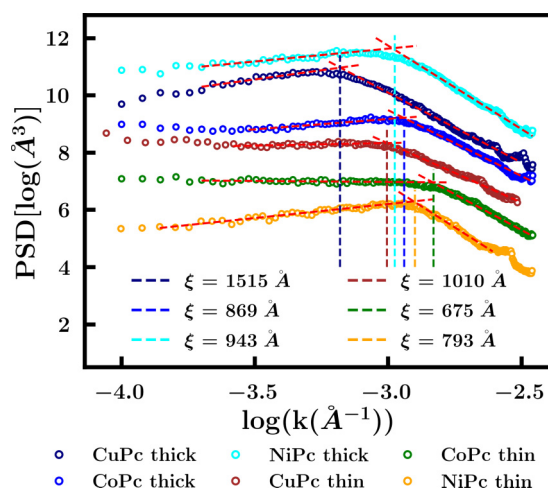


FIG. 5. PSD profile of AFM images of Fig. 4. Open circles denotes the data and red-dashed lines are corresponding linear fit. The in-plane correlation lengths  $\xi$  are shown from the specific positions of the wavevector  $k$  (marked by dashed lines of corresponding color) are indicated.

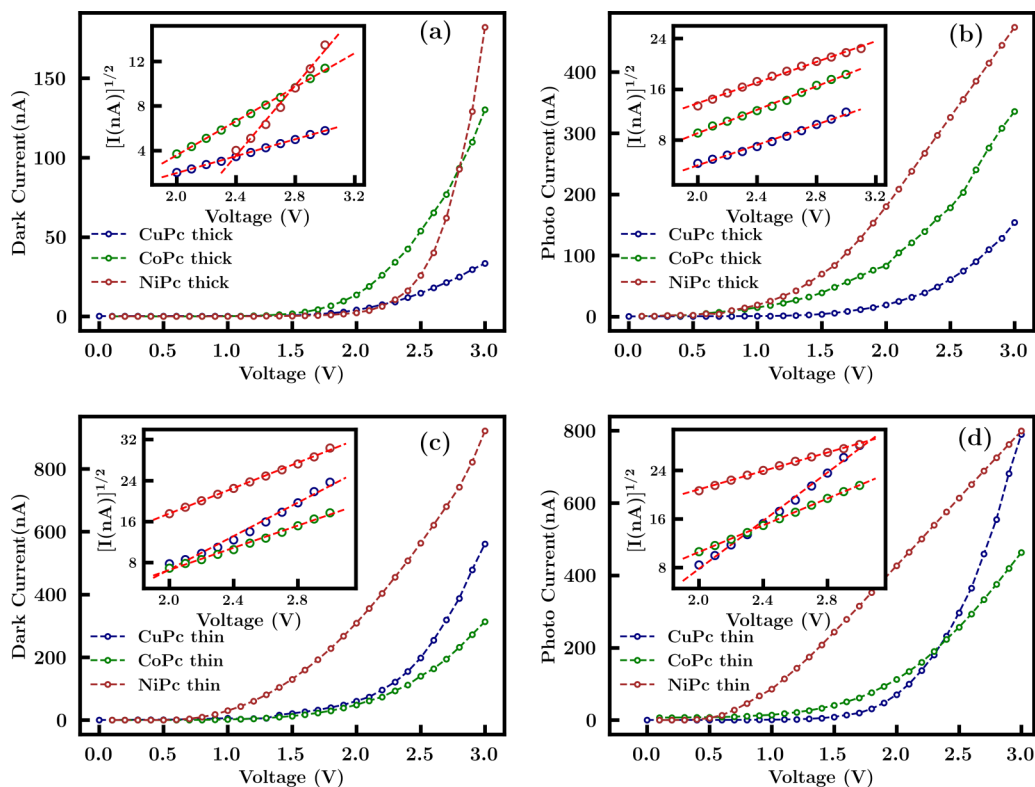


FIG. 6. (a) and (c) show the  $I$ - $V$  characteristics under dark condition of thick and thin films, respectively. (b) and (d) show the  $I$ - $V$  characteristics under UV illumination condition of thick and thin films respectively. Corresponding  $\sqrt{I}$  vs  $V$  plot in insets.

PSD, directly to a real space length [58,59]. The obtained correlation lengths  $\xi$  from the PSD curves have been indicated by the dashed line in the PSD profile (Fig. 5). Here we have fitted each PSD curve with two straight lines and used the  $k$  values of the intersection points to estimate the corresponding  $\xi$  values. It is interesting to note that the obtained lengths from the PSD curves match well with the interstick distance obtained from the GISAXS analysis.

We have also taken SEM images for three types of films, shown in Figs. 4(g)–4(i). The images are not sharp due to very low-density contrast in the fully covered surface region. Images taken from the edges of the films are shown in the corresponding insets. These inset images are shown to represent the molecular assembly shape with better clarity. We can see that each of these images consists of sticklike shaped molecular assembly which are randomly distributed over the substrate. This observation justifies our model of 1D sticks considered to fit the GISAXS profiles.

The charge carrier transport through such organic semiconductor materials is vastly affected by the trapped charge-carrier states of the material [60–63]. To understand the correlation of such crystalline and porous domain structures for the development of the trap states in carrier transport, we have measured the  $I$ - $V$  characteristics for thin (B) and thick (D) samples as shown in Fig. 6. We have performed the experiment in dark conditions and as well as under UV illumination and the corresponding current is referred to as “dark current” and “photo current,” respectively. We can see that the value of photo current is significantly high for all the thick samples under UV illumination in comparison to the

respective dark currents. But this difference in values of dark current and photo current is much lower for the thinner samples as shown in Figs. 6(c) and 6(d). In fact, it was observed that the photo-current value of thick samples is comparable to the values of dark current of thin samples, i.e., an increase in the thickness of the films results in a more resistive path contrary to the normal circumstances. After a certain voltage (threshold  $V_{th}$ ), the current is found to be nonlinear for all the samples. The value of  $V_{th}$  for all three materials also decreases with decreasing thickness under UV illumination. The  $\sqrt{I}$  vs  $V$  plot for all the samples follows a straight line at high voltage region as shown in the insets of Fig. 6. This  $V^2$  dependence of current implies that the current through the material of the film is bulk trapped which corresponds to the space-charge limited conduction (SCLC) [60,61]. It is known that these trap states are generally situated in the band gap of the material and when the applied voltage exceeds the value of the barrier corresponding to the trapped states then the current increases rapidly with voltage resulting in such  $V^2$  dependence [62]. Under illumination conditions, the Fermi level rises and the trap carrier states become more populated with charge carriers, thus the newly injected charge carriers are not getting trapped further. Therefore, the free carrier increases, which results in a lowering of the  $V_{th}$  and a rapid increase of current with applied voltage. The defects or voids produced between the crystalline and noncrystalline domains due to spontaneous aggregation of molecules during the film growth process [64] can be responsible for the decrease in in-plane conductivity with an increase in thickness of the film. As the columnar structure evolves with an increase

in thickness, the molecular realignment with the crystalline domains may leave some voids between the crystalline and noncrystalline regions, leading to a decrease in number of possible paths for charge transport through the materials. This transition makes the material more resistive, resulting in a decrease in current for thick films. The GISAXS data shows the increase in crystalline size and intercrystalline domain distance with an increasing thickness that supports the proposed mechanism for the existence of extra resistance in the thick films.

#### IV. CONCLUSION

The structure-property correlation in thin films of small organic semiconductor molecules is very important for the wide range of applications of these materials as devices. Here, we have investigated the growth and structural evolution of three different metal (Cu, Co, and Ni) Pc molecules in thin films and explained the differences in charge-carrier transport in thick and thin films with the structural organization of the molecules in the film. The XRR of CuPc films show clear Kiessig oscillations corresponding to uniform film thickness, and almost undamped Laue oscillation around the Bragg peak. This indicates a coherently ordered out-of-plane structure of CuPc molecular periodicity in the vertical direction on Si substrate. The Laue oscillations are not so prominent for CoPc and NiPc thin films but higher thickness films show similar out-of-plane ordering as found for the CuPc molecules. The in-plane structure reveals a two-dimensional arrangement of sticklike crystalline ordered assembly formed by the Pc molecules. The surface morphology imaged from AFM and SEM also shows the similar ordered structure in thin-film configuration. The interstick distances increase with thickness

for all the molecules but the increase is more for CuPc molecules and the least in NiPc molecules. The PSD profile analysis also corroborates this observation. The in-plane  $I$ - $V$  characteristics measured on thin and thick samples show higher current for the thinner samples than the thick samples in contrast to the normal circumstances. The appearance of defects or trapped states due to molecular realignment results in extra resistance and affects the charge-carrier transport through the thick materials. Though hopping-mediated transport is the primary mode of transport in such OSC materials, here the contribution to transport of charge carriers is more dominated by the trap states of the crystalline domains. The investigation of structural configuration of such small organic molecules in thin films helped us to solve the discrepancies in charge transport through the materials as a function of film thickness.

#### ACKNOWLEDGMENTS

The authors acknowledge Dr. Gouranga Manna for GISAXS, Mr. Debraj Dey for SEM, and Mr. Saugata Roy and Subhankar Mandal for AFM measurement. The authors also acknowledge Ms. Mousri Paul and Ms. Pooja Agarwal for their help in device fabrication. Authors thank the Department of Science and Technology, India, for the financial support and Jawaharlal Nehru Centre for Advanced Scientific Research, Bangalore, India, for facilitating the experiments at the Indian Beamline, Photon Factory, KEK, Japan. S.K. also acknowledge University Grant Commission (UGC) for providing financial assistance. M.K.S. acknowledges the support of Indian National Science Academy Senior Scientist Programme.

- 
- [1] Y. Zhou, S.-T. Han, Y. Yan, L.-B. Huang, L. Zhou, J. Huang, and V. A. L. Roy, Solution processed molecular floating gate for flexible flash memories, *Sci. Rep.* **3**, 3093 (2013).
  - [2] S. Park, Z. Liao, B. Ibarlucea, H. Qi, H.-H. Lin, D. Becker, J. Melidonie, T. Zhang, H. Sahabudeen, L. Baraban, C.-K. Baek, Z. Zheng, E. Zschech, A. Fery, T. Heine, U. Kaiser, G. Cuniberti, R. Dong, and X. Feng, Two-dimensional boronate ester covalent organic framework thin films with large single crystalline domains for a neuromorphic memory device, *Angew. Chem. Int. Ed.* **59**, 8218 (2020).
  - [3] S. Ding, Y. Tian, Y. Li, H. Zhang, K. Zhou, J. Liu, L. Qin, X. Zhang, X. Qiu, H. Dong, D. Zhu, and W. Hu, Organic single-crystal spintronics: Magnetoresistance devices with high magnetic-field sensitivity, *ACS Nano* **13**, 9491 (2019).
  - [4] F.-J. Meyer zu Heringdorf, M. C. Reuter, and R. M. Tromp, Growth dynamics of pentacene thin films, *Nature (London)* **412**, 517 (2001).
  - [5] S. Lee, B. Koo, J.-G. Park, H. Moon, J. Hahn, and J. M. Kim, Development of high-performance organic thin-film transistors for large-area displays, *MRS Bull.* **31**, 455 (2006).
  - [6] A. Dodabalapur, H. E. Katz, L. Torsi, and R. C. Haddon, Organic field-effect bipolar transistors, *Appl. Phys. Lett.* **68**, 1108 (1996).
  - [7] A. Dodabalapur, H. E. Katz, L. Torsi, and R. C. Haddon, Organic heterostructure field-effect transistors, *Science* **269**, 1560 (1995).
  - [8] R. R. Cranston and B. H. Lessard, Metal phthalocyanines: thin-film formation, microstructure, and physical properties, *RSC Adv.* **11**, 21716 (2021).
  - [9] A. Babel, J. Wind, and S. Jenekhe, Ambipolar charge transport in air-stable polymer blend thin-film transistors, *Adv. Funct. Mater.* **14**, 891 (2004).
  - [10] J. Zaumseil, R. H. Friend, and H. Sirringhaus, Spatial control of the recombination zone in an ambipolar light-emitting organic transistor, *Nat. Mater.* **5**, 69 (2006).
  - [11] Z. H. Xiong, D. Wu, Z. Vally Vardeny, and J. Shi, Giant magnetoresistance in organic spin-valves, *Nature (London)* **427**, 821 (2004).
  - [12] G. O. N. Ndjawa, K. R. Graham, R. Li, S. M. Conron, P. Erwin, K. W. Chou, G. F. Burkhard, K. Zhao, E. T. Hoke, M. E. Thompson *et al.*, Impact of molecular orientation and spontaneous interfacial mixing on the performance of organic solar cells, *Chem. Mater.* **27**, 5597 (2015).
  - [13] A. L. Ayzner, D. Nordlund, D.-H. Kim, Z. Bao, and M. F. Toney, Ultrafast electron transfer at organic semiconductor interfaces: Importance of molecular orientation, *J. Phys. Chem. Lett.* **6**, 6 (2015).

- [14] H.-C. Lin, G. A. MacDonald, Y. Shi, N. W. Polaske, D. V. McGrath, S. R. Marder, N. R. Armstrong, E. L. Ratcliff, and S. S. Saavedra, Influence of molecular orientation on charge-transfer processes at phthalocyanine/metal oxide interfaces and relationship to organic photovoltaic performance, *J. Phys. Chem. C* **119**, 10304 (2015).
- [15] B. P. Rand, D. Cheyens, K. Vasseur, N. C. Giebink, S. Mothy, Y. Yi, V. Coropceanu, D. Beljonne, J. Cornil, J.-L. Brédas *et al.*, The impact of molecular orientation on the photovoltaic properties of a phthalocyanine/fullerene heterojunction, *Adv. Funct. Mater.* **22**, 2987 (2012).
- [16] E. Suito, N. Uyeda, and M. Ashida, Epitaxial growth of condensed aromatic polycyclic compounds, *Nature (London)* **194**, 273 (1962).
- [17] T. Nonaka, Y. Nakagawa, Y. Mori, M. Hirai, T. Matsunobe, M. Nakamura, T. Takahagi, A. Ishitani, H. Lin, and K. Koumoto, Epitaxial growth of  $\alpha$ -copper phthalocyanine crystal on Si(001) substrate by organic molecular beam deposition, *Thin Solid Films* **256**, 262 (1995).
- [18] M. Nakamura, Y. Morita, Y. Mori, A. Ishitani, and H. Tokumoto, Molecular arrangement of copper phthalocyanine on hydrogen-terminated Si(111): Influence of surface roughness, *J. Vac. Sci. Technol. B* **14**, 1109 (1996).
- [19] R. Hiesgen, M. Rübisch, H. Böttcher, and D. Meissner, STM investigation of the growth structure of Cu-phthalocyanine films with submolecular resolution, *Sol. Energy Mater. Sol. Cells* **61**, 73 (2000).
- [20] O. Berger, W.-J. Fischer, B. Adolph, S. Tierbach, V. Melev, and J. Schreiber, Studies on phase transformations of Cu-phthalocyanine thin films, *J. Mater. Sci.: Mater. Electron.* **11**, 331 (2000).
- [21] H. X. Wei, J. Li, Z. Q. Xu, Y. Cai, J. X. Tang, and Y. Q. Li, Thermal annealing-induced vertical phase separation of copper phthalocyanine: Fullerene bulk heterojunction in organic photovoltaic cells, *Appl. Phys. Lett.* **97**, 083302 (2010).
- [22] P. Peumans, S. Uchida, and S. R. Forrest, Efficient bulk heterojunction photovoltaic cells using small-molecular-weight organic thin films, *Nature (London)* **425**, 158 (2003).
- [23] F. Yang, K. Sun, and S. Forrest, Efficient solar cells using all-organic nanocrystalline networks, *Adv. Mater.* **19**, 4166 (2007).
- [24] J. W. Kim, H. J. Kim, H. H. Lee, T. Kim, and J.-J. Kim, Formation of bulk heterojunctions by alternative thermal deposition and its structure analysis for high efficiency small molecular organic photovoltaics, *Adv. Funct. Mater.* **21**, 2067 (2011).
- [25] B. Reisz, E. Empting, M. Zwadlo, M. Hodas, G. Duva, V. Belova, C. Zeiser, J. Hagenlocher, S. Maiti, A. Hinderhofer, A. Gerlach, M. Oettel, and F. Schreiber, Thin film growth of phase-separating phthalocyanine-fullerene blends: A combined experimental and computational study, *Phys. Rev. Mater.* **5**, 045601 (2021).
- [26] A. A. Virkar, S. Mannsfeld, Z. Bao, and N. Stingelin, Organic semiconductor growth and morphology considerations for organic thin-film transistors, *Adv. Mater.* **22**, 3857 (2010).
- [27] P. Kumar, A. Sharma, S. Yadav, and S. Ghosh, Morphology optimization for achieving air stable and high performance organic field effect transistors, *Org. Electron.* **14**, 1663 (2013).
- [28] V. Rani, A. Sharma, P. Kumar, B. Singh, and S. Ghosh, Charge transport mechanism in copper phthalocyanine thin films with and without traps, *RSC Adv.* **7**, 54911 (2017).
- [29] S. Pachmajer, A. O. F. Jones, M. Truger, C. Röthel, I. Salzmann, O. Werzer, and R. Resel, Self-limited growth in pentacene thin films, *ACS Appl. Mater. Interfaces* **9**, 11977 (2017).
- [30] M. R. Kiran, H. Ulla, M. Satyanarayan, and G. Umesh, Effect of deposition rate on the charge transport in Vanadyl-phthalocyanine thin films, *Synth. Met.* **224**, 63 (2017).
- [31] K. Onlaor, B. Tunhoo, P. Keeratithiwakorn, T. Thiawong, and J. Nukeaw, Electrical bistable properties of copper phthalocyanine at different deposition rates, *Solid-State Electron.* **72**, 60 (2012).
- [32] R. Resel, M. Ottmar, M. Hanack, J. Keckes, and G. Leising, Preferred orientation of copper phthalocyanine thin films evaporated on amorphous substrates, *J. Mater. Res.* **15**, 934 (2000).
- [33] H. J. Kim, J. W. Kim, H. H. Lee, T.-M. Kim, J. Jang, and J.-J. Kim, Grazing incidence small-angle x-ray scattering analysis of initial growth of planar organic molecules affected by substrate surface energy, *J. Phys. Chem. Lett.* **2**, 1710 (2011).
- [34] K. Xiao, Y. Liu, G. Yu, and D. Zhu, Influence of the substrate temperature during deposition on film characteristics of copper phthalocyanine and field-effect transistor properties, *Appl. Phys. A* **77**, 367 (2003).
- [35] S.-C. Suen, W.-T. Whang, F.-J. Hou, and B.-T. Dai, Low-temperature self-assembly of copper phthalocyanine nanofibers, *Org. Electron.* **7**, 428 (2006).
- [36] S. Khodabakhsh, B. Sanderson, J. Nelson, and T. Jones, Using self-assembling dipole molecules to improve charge collection in molecular solar cells, *Adv. Funct. Mater.* **16**, 95 (2006).
- [37] Y.-S. Hsiao, W.-T. Whang, S.-C. Suen, J.-Y. Shiu, and C.-P. Chen, Morphological control of CuPc and its application in organic solar cells, *Nanotechnology* **19**, 415603 (2008).
- [38] S. R. Forrest, Ultrathin organic films grown by organic molecular beam deposition and related techniques, *Chem. Rev.* **97**, 1793 (1997).
- [39] T. L. Derrien, A. E. Lauritzen, P. Kaienburg, E. Hancox, C. Nicklin, and M. Riede, Interfacial rearrangements and strain evolution in the thin film growth of ZnPc on glass, *Phys. Rev. Mater.* **6**, 033401 (2022).
- [40] D. R. Tackley, G. Dent, and W. E. Smith, Phthalocyanines: structure and vibrations, *Phys. Chem. Chem. Phys.* **3**, 1419 (2001).
- [41] M. Szybowicz, W. Bała, K. Fabisiak, K. Paprocki, and M. Drozdowski, The molecular structure ordering and orientation of the metallophthalocyanine CoPc, ZnPc, CuPc, and MgPc thin layers deposited on silicon substrate, as studied by micro-Raman spectroscopy, *J. Mater. Sci.* **46**, 6589 (2011).
- [42] M. Szybowicz and J. Makowiecki, Orientation study of iron phthalocyanine (FePc) thin films deposited on silicon substrate investigated by atomic force microscopy and micro-Raman spectroscopy, *J. Mater. Sci.* **47**, 1522 (2012).
- [43] I. Bruder, J. Schöneboom, R. Dinnebier, A. Ojala, S. Schäfer, R. Sens, P. Erk, and J. Weis, What determines the performance of metal phthalocyanines (MPc, M=Zn, Cu, Ni, Fe) in organic heterojunction solar cells? A combined experimental and theoretical investigation, *Org. Electron.* **11**, 377 (2010).
- [44] M.-S. Liao and S. Scheiner, Electronic structure and bonding in metal phthalocyanines, Metal=Fe, Co, Ni, Cu, Zn, Mg, *J. Chem. Phys.* **114**, 9780 (2001).
- [45] M. K. Sanyal, M. K. Mukhopadhyay, M. Mukherjee, A. Datta, J. K. Basu, and J. Penfold, Role of molecular self-assembling

- in Langmuir-Blodgett film growth, *Phys. Rev. B* **65**, 033409 (2002).
- [46] L. G. Parratt, Surface studies of solids by total reflection of x-rays, *Phys. Rev.* **95**, 359 (1954).
- [47] X. Ai, J. Lin, Y. Chang, L. Zhou, X. Zhang, and G. Qin, Phase modification of copper phthalocyanine semiconductor by converting powder to thin film, *Appl. Surf. Sci.* **428**, 788 (2018).
- [48] X. Ji, T. Zou, H. Gong, Q. Wu, Z. Qiao, W. Wu, and H. Wang, Cobalt phthalocyanine nanowires: Growth, crystal structure, and optical properties, *Cryst. Res. Technol.* **51**, 154 (2016).
- [49] J. Song, X. Wang, J. Liao, W. Zhou, J. Song, Z. Zhao, L. Zhang, E. Joselevich, and J. Xu, Horizontally-oriented growth of organic crystalline nanowires on polymer films for *in situ* flexible photodetectors with Vis-NIR response and high bending stability, *Adv. Funct. Mater.* **33**, 2213888 (2023).
- [50] B. Reisz, V. Belova, G. Duva, C. Zeiser, M. Hodas, J. Hagara, P. Šiffalovič, L. Pithan, T. Hosokai, A. Hinderhofer, A. Gerlach, and F. Schreiber, Polymorphism and structure formation in copper phthalocyanine thin films, *J. Appl. Crystallogr.* **54**, 203 (2021).
- [51] C. Frank, R. Banerjee, M. Oettel, A. Gerlach, J. Novák, G. Santoro, and F. Schreiber, Analysis of island shape evolution from diffuse x-ray scattering of organic thin films and implications for growth, *Phys. Rev. B* **90**, 205401 (2014).
- [52] F. Leroy, R. Lazzari, and G. Renaud, Effects of near-neighbor correlations on the diffuse scattering from a one-dimensional paracrystal, *Acta Crystallogr. Sect. A* **60**, 565 (2004).
- [53] D. Babonneau, S. Camelio, E. Vandenhecke, S. Rousselet, M. Garel, F. Pailloux, and P. Boesecke, Quantitative analysis of nanoripple and nanoparticle patterns by grazing incidence small-angle x-ray scattering 3D mapping, *Phys. Rev. B* **85**, 235415 (2012).
- [54] Y.-P. Zhao, I. Wu, C.-F. Cheng, U. Block, G.-C. Wang, and T.-M. Lu, Characterization of random rough surfaces by in-plane light scattering, *J. Appl. Phys.* **84**, 2571 (1998).
- [55] Y. Zhang, E. Barrena, X. Zhang, A. Turak, F. Maye, and H. Dosch, New insight into the role of the interfacial molecular structure on growth and scaling in organic heterostructures, *J. Phys. Chem. C* **114**, 13752 (2010).
- [56] Y. Zhao, G.-C. Wang, and T.-M. Lu, *Characterization of Amorphous and Crystalline Rough Surface—Principles and Applications* (Elsevier, San Diego, 2000).
- [57] S. M. Obaidulla and P. K. Giri, Surface roughening and scaling behavior of vacuum-deposited SnCl<sub>2</sub>Pc organic thin films on different substrates, *Appl. Phys. Lett.* **107**, 221910 (2015).
- [58] A. Hinderhofer, A. Gerlach, S. Kowarik, F. Zontone, J. Krug, and F. Schreiber, Smoothing and coherent structure formation in organic-organic heterostructure growth, *Europhys. Lett.* **91**, 56002 (2010).
- [59] S. Yim and T. S. Jones, Anomalous scaling behavior and surface roughening in molecular thin-film deposition, *Phys. Rev. B* **73**, 161305(R) (2006).
- [60] Z. Wang, Y. Lou, S. Naka, and H. Okada, Bias and temperature dependent charge transport in solution-processed small molecular mixed single layer organic light emitting devices, *Appl. Phys. Lett.* **98**, 063302 (2011).
- [61] A. J. Campbell, M. S. Weaver, D. G. Lidzey, and D. D. C. Bradley, Bulk limited conduction in electroluminescent polymer devices, *J. Appl. Phys.* **84**, 6737 (1998).
- [62] Y.-H. Lou, L. Zhang, M.-F. Xu, Z.-K. Wang, S. Naka, H. Okada, and L.-S. Liao, Direct comparison of charge transport and electronic traps in polymer-fullerene blends under dark and illuminated conditions, *Org. Electron.* **15**, 299 (2014).
- [63] C. N. Colesniuc, R. R. Biswas, S. A. Hevia, A. V. Balatsky, and I. K. Schuller, Exponential behavior of the Ohmic transport in organic films, *Phys. Rev. B* **83**, 085414 (2011).
- [64] G. Yoshikawa, J. T. Sadowski, A. Al-Mahboob, Y. Fujikawa, T. Sakurai, Y. Tsuruma, S. Ikeda, and K. Saiki, Spontaneous aggregation of pentacene molecules and its influence on field effect mobility, *Appl. Phys. Lett.* **90**, 251906 (2007).